International Journal of Solids and Structures 46 (2009) 1326–1333

Contents lists available at ScienceDirect

International Journal of Solids and Structures

journal homepage: www.elsevier.com/locate/ijsolstr

Kinetics of smart hydrogels responding to electric field: A transient deformation analysis

Hua Li *

School of Mechanical and Aerospace Engineering, Nanyang Technological University, 50 Nanyang Avenue, Singapore 639798, Republic of Singapore

ARTICLE INFO

Article history:
Received 4 March 2008
Received in revised form 15 September 2008
Available online 12 November 2008

Keywords:
Kinetics
Smart hydrogel
Electric stimulus
Modeling
Transient deformation

ABSTRACT

A multiphysics model is presented in this paper for simulation of kinetics of the smart hydrogels subject to an externally applied electric field, especially for analysis of the transient deformation of the hydrogel. The model termed the multi-effect-coupling electric stimulus (MECe) takes account of the coupled chemo-electro-mechanical multiphysics domains and the multi-phase effect of polymeric network and interstitial liquid as well as ionic species. The MECe model is validated well by transient simulation and comparison with available experimental data. Kinetics of ionic concentration of diffusive species is simulated. Parameter studies on the hydrogel displacement are conducted in detail for influences of externally applied electric voltage, initially fixed-charge density and surrounding bath solution concentration.

1. Introduction

In general, hydrogel is a hydrophilic multi-phase mixture, which is composed of three-dimensional cross-linked polymeric network matrix solid phase and interstitial liquid phase. This makes the hydrogel behave both solid-like and liquid-like properties. If an ionic monomer is incorporated into the polymeric network, usually the hydrogel can respond to environmental stimuli and then it is called the smart hydrogel, in which the charged group is formed and termed fixed-charge since its mobility is much less than that of freely mobile ionic species within the interstitial liquid, as shown in Fig. 1.

It is well known that the smart hydrogels have wide range of applications in bioengineering areas, where they are used as active element in BioMEMS for controlled drug release, micro-scale actuating/sensing, micro-fluidic flow control and filtration/separation (Galaev and Mattiasson, 1999; Beebe et al., 2000; Jeong and Gutowska, 2002), due to their sensitivity to a large variety of environmental stimuli such as electric field, solution pH, temperature and chemicals (Tanaka, 1978; Tanaka et al., 1980; Tanaka et al., 1982; Siegel and Firestone, 1988; Kwon et al., 1991; Kokufuta et al., 1991; Osada et al., 1992; Chen and Hoffman, 1995; Yoshida et al., 1995; Kataoka et al., 1998).

So far the mechanism of the smart hydrogels responding to electric voltage has still remained poorly understood although many experimental and theoretical investigations of the hydrogels were conducted. Few studies of theoretical modeling are found in open literature. They include the early bi-phase model developed by Mow et al. (1980), the swelling thermo-analog theory by Myers et al. (1984), the bi-component theory by Lanir (1987) and the electromechanical theory by Eisenberg and Grodzinsky (1987). In general, it is difficult for these models to work well because they exclude several important physical parameters such as the fixed-charge density and diffusive ionic concentrations. In order to overcome the drawbacks, a tri-phase mechano-electrochemical model was proposed by Lai et al. (1991) for analysis of the response of hydrogel-like tissues by incorporating the chemical potential whose gradient is considered as driving force for fluid flow and ion transport. Wallmersperger et al. (2004) and Zhou et al. (2002) put forward the models for deformation of the electric-sensitive hydrogels subject to external electric field. However, the models still have limited applications. For example, Wallmersperger et al. (2004) directly used Newton's second law as mechanical governing equation, resulting in difficulty to describe the mechanical behavior of multi-phase hydrogels. In the model by Zhou et al. (2002), the electro-neutrality condition is required, and simulated domain is limited within interior hydrogel only, excluding the surrounding bath solution. For further improvement of theoretical modeling of the electric-sensitive hydrogels, the present author has developed a multiphysics model consisting of coupled nonlinear partial differential governing equations (Li et al., 2004c), which is based on the multi-phase theory and termed the multi-effect-coupling electric-stimulus (MECe) model, for simulation of responsive behaviors of the smart hydrogels when immersed into bath solution subject to externally applied electric field. Computational

* Tel.: +65 6790 4953; fax: +65 6792 4062/6791 1859.
E-mail addresses: lihua@ntu.edu.sg, lihua@ihpc.a-star.edu.sg.

0020-7683/$ - see front matter © 2008 Elsevier Ltd. All rights reserved.
doi:10.1016/j.ijsolstr.2008.11.001

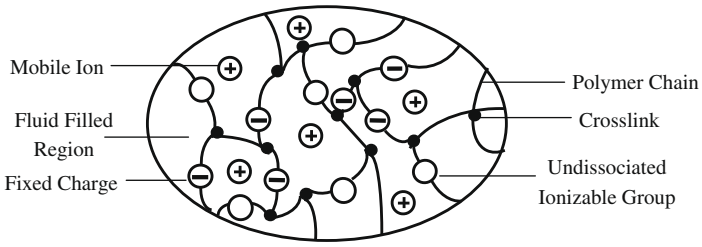

Fig. 1. Microscopic structure of the charged hydrogel.

accuracy of the MECe model has been validated in steady-state simulation to predict the equilibrium of the hydrogels (Li et al., 2004a).

In this paper, the MECe model will be further examined in transient simulation for kinetics of the hydrogels. The model is discretized first and then numerical simulation is compared with published experimental data. The transient simulations are conducted for analysis of the concentration kinetics of ionic species and the influence of several important parameters on the displacement of the electric-stimulus responsive hydrogels. The parameters include externally applied electric voltage, initially fixed-charge density and surrounding bath solution concentration.

2. Formulation of MECe model

2.1. Transient governing equations of the MECe model

Formulation of the MECe model is based on the two assumptions: (a) the smart hydrogel is immersed in an unstirred solution in vibration-free experimental device; the bulk flow of fluid or hydrodynamic velocity can thus be eliminated and subsequently the convective flux is neglected and (b) the pore of the present hydrogel is narrow enough and thus the diffusion dominates the transmission of flux. The governing equations of the MECe model are composed of (Li et al., 2004a,c)

(a) Nernst–Planck equation for the concentration c^k of the kth diffusive ion species

$$\frac{\partial c_k}{\partial t} = (D_k c^k_{,i})_{,i} + \frac{F_c z^k}{RT}(D_k c^k \psi_{,i})_{,i} \quad (k = 1, 2, \ldots n_f) \tag{1}$$

(b) Poisson equation for the electric potential ψ,

$$\nabla^2 \psi = -\frac{F_c}{\varepsilon \varepsilon_0} \sum_{k=1}^{n_f} (z^k c^k + z^f c^f) \tag{2}$$

(c) the continuity and momentum equations of the mixture for the fluid pressure p and displacement u of the hydrogel,

$$\nabla \frac{\partial u}{\partial t} = \nabla \left[\frac{(\phi^w)^2}{f_{ws}} \left(\nabla p + RT \nabla \sum_k (1 - \Phi^k) c^k + F_c \sum_k z^k c^k \nabla \psi \right) \right] \tag{3}$$

$$\nabla \cdot (-p\mathrm{I} + \lambda_s tr(E)\mathrm{I} + 2\mu_s E) = 0 \tag{4}$$

(d) the constitutive equation of the fixed-charge density c^f and the volume fraction ϕ^w of water phase,

$$c^f = \frac{c_0^f}{(1 + tr(E)/\phi_0^w)}, \quad \phi^w = 1 - \frac{\phi_0^s}{(1 + tr(E))} \tag{5}$$

where D_k, c^k and z^k are the diffusive coefficient, concentration and valance of the kth ion species, respectively. F_c is the Faraday constant, R is the universal gas constant, T is the absolute temperature, ψ is the electric potential, ε is the dielectric constant and ε_0 is the permittivity of free space. c^f and z^f are the density and valence of the fixed-charge group. ϕ^w is the volume fraction of water phase, f_{ws} is the diffusive drag coefficient between the polymeric matrix solid and interstitial water phases, Φ^k is the osmotic coefficient of the kth ion species and p is the fluid pressure. u and $\boldsymbol{E}$ are the displacement and elastic strain vector of the polymeric solid matrix. λ_s and μ_s are Lamé coefficients of the matrix. c_0^f, ϕ_0^s and ϕ_0^w are the fixed-charge density and volume fractions of solid and water phases at a reference configuration, respectively, where the reference configuration is defined as the equilibrium state of the studied system when the hydrogel is immersed in the bath solution without the externally applied electric field.

For simplification of numerical simulation, six non-dimensional variables are defined as follows:

$$\bar{\zeta} = \frac{\zeta}{L_{ref}} \quad \bar{u} = \frac{u}{L_{ref}} \tag{6}$$

$$\bar{c}_k = \frac{c_k}{c_{ref}} \quad \bar{c}_f = \frac{c_f}{c_{ref}} \tag{7}$$

$$\bar{\psi} = \frac{\psi}{\psi_{ref}} = \frac{F\psi}{\alpha RT} \tag{8}$$

$$\bar{p} = \frac{p}{p_{ref}} = \frac{p}{\beta c_{ref} RT} \tag{9}$$

where ζ denotes spatial coordinate variable. α and β are non-dimensional adjustable parameters, which are introduced for more flexible simulating regions of the electric potential ψ and fluid pressure p.

By substituting the non-dimensional variables defined in (6)–(9) into the MECe transient governing equations (1)–(4), we derive the non-dimensional form of the MECe model as

$$L_{ref}^2 \frac{\partial \bar{c}_k}{\partial t} = (D_k \bar{c}^k_{,i})_{,i} + \alpha z^k (D_k \bar{c}^k \bar{\psi}_{,i})_{,i} \quad (k = 1, 2, \ldots, n_f) \tag{10}$$

$$\nabla^2 \bar{\psi} = -\frac{F_c^2 L_{ref}^2 c_{ref}}{\varepsilon \varepsilon_0 RT \alpha} \sum_{k=1}^{n_f} (z^k \bar{c}^k + z^f \bar{c}^f) \tag{11}$$

$$\frac{L_{ref}^2}{c_{ref} RT} \nabla \frac{\partial \bar{u}}{\partial t} = \nabla \left[\frac{(\phi^w)^2}{f_{ws}} (\beta \nabla \bar{p} + RT \nabla \sum_k (1 - \Phi^k) \bar{c}^k + \alpha \sum_k z^k \bar{c}^k \nabla \bar{\psi}) \right] \tag{12}$$

$$\beta RT c_{ref} \nabla \cdot (p\mathrm{I}) = \nabla (\lambda_s tr(E)\mathrm{I} + 2\mu_s E) \tag{13}$$

One-dimensional transient numerical simulations as preliminary study are conducted in this paper. As shown in Fig. 2, an electric-sensitive hydrogel strip is placed into the ideal NaCl solution subject to an externally applied electric field. Displacement along the x direction is computed here. It is assumed in this paper that one of two edge points a and b in the thickness h direction is fixed to eliminate the rigid-body displacement of the hydrogel strip. The governing equations (10)–(13) of MECe model are thus reduced to the 1D non-dimensional partial differential transient equations as follows:

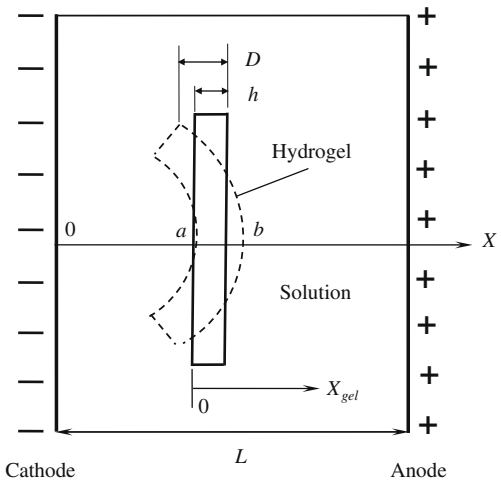

Fig. 2. Diagram of a hydrogel strip immersed in bath solution under applied electric field, where the whole computational domain is defined as the *X*-coordinate system and the hydrogel domain as the *X gel*-coordinate system.

$$L_{ref}^2\frac{\partial \bar{c}^k}{\partial t}=D_k\left(\frac{\partial^2 \bar{c}^k}{\partial \bar{x}^2}+\alpha z^k\frac{\partial \bar{c}^k}{\partial \bar{x}}\frac{\partial \bar{\psi}}{\partial \bar{x}}+\alpha z^k\bar{c}^k\frac{\partial^2 \bar{\psi}}{\partial \bar{x}^2}\right)\quad (k=+,-) \tag{14}$$

$$\frac{\partial^2 \bar{\psi}}{\partial \bar{x}^2}+\frac{F_c^2L_{ref}^2c_{ref}}{\varepsilon\varepsilon_0RT\alpha}\left(\sum_{k=+,-}z^k\bar{c}^k+z^f\bar{c}^f\right)=0 \tag{15}$$

$$(3\lambda_s+2\mu_s)\frac{\partial^2 \bar{u}}{\partial \bar{x}^2}-\beta RTc_{ref}\frac{\partial \bar{p}}{\partial \bar{x}}=0 \tag{16}$$

$$\begin{aligned}\frac{L_{ref}^2f_{ws}}{c_{ref}RT}\frac{\partial}{\partial t}\left(\frac{\partial \bar{u}}{\partial \bar{x}}\right)&=\beta\left(\phi^w\frac{\partial^2 \bar{p}}{\partial \bar{x}^2}+2\frac{\partial \phi^w}{\partial \bar{x}}\frac{\partial \bar{p}}{\partial \bar{x}}\right)\\&+\alpha\left[2\frac{\partial \phi^w}{\partial \bar{x}}\frac{\partial \bar{\psi}}{\partial \bar{x}}\sum_{k=+,-}z^k\bar{c}^k+\phi^w\left(\frac{\partial \bar{\psi}}{\partial \bar{x}}\sum_{k=+,-}\left(z^k\frac{\partial \bar{c}^k}{\partial \bar{x}}\right)\right.\right.\\&\left.\left.+\frac{\partial^2 \bar{\psi}}{\partial \bar{x}^2}\sum_{k=+,-}z^k\bar{c}^k\right)\right]\end{aligned} \tag{17}$$

2.2. Boundary and initial conditions

The computational domain of Eqs. (14) and (15) is defined as covering both the hydrogel and surrounding bath solution for the ionic concentrations $\bar{c}^k$ and electric potential $\bar{\psi}$. As such, the boundary conditions of the unknown $\bar{c}^k$ and $\bar{\psi}$ are imposed at the two electrodes located at the ends of bath solution as illustrated in Fig. 2,

$$\bar{c}|_{Anode}=\bar{c}|_{Cathode}=\bar{c}^* \tag{18}$$

$$\bar{\psi}|_{Anode}=0.5\overline{V}_e\quad\text{and}\quad\bar{\psi}|_{Cathode}=-0.5\overline{V}_e \tag{19}$$

where $\bar{c}^*$ is the initial concentration of the bath salt solution and $\overline{V}_e$ is the applied voltage.

For the fluid pressure $\bar{p}$ and hydrogel displacement $\bar{u}$ however, the computational domain of Eqs. (16) and (17) covers the hydrogel region only. The corresponding boundary conditions are required at both the interfaces between the hydrogel and surrounding solution. It is assumed in an equilibrium state that the chemical potentials of fluid and ion phases inside the hydrogels should be equal to those outside the hydrogels. As such, the boundary condition of the fluid pressure $\bar{p}$ at the hydrogel–solution interfaces is given as (Li et al., 2007)

$$\begin{aligned}\bar{p}_{\text{interface}}=RT(&\bar{c}^+_{\text{in}-\text{interface}}+\bar{c}^-_{\text{in}-\text{interface}}-\bar{c}^+_{\text{out}-\text{interface}}\\&-\bar{c}^-_{\text{out}-\text{interface}})-p_0\end{aligned} \tag{20}$$

where $\bar{c}^k_{\text{in}-\text{interface}}$ and $\bar{c}^k_{\text{out}-\text{interface}}$ ($k=+,-$) are the ionic concentrations within the hydrogels near the interfaces and within the bath solution near the interfaces, respectively. p_0 denotes the surrounding fluid pressure at reference configuration. In state of the mechanical equilibrium of the hydrogels, the boundary condition of the displacement $\bar{u}$ at the hydrogel–solution interface may be written as

$$(3\lambda_s+2\mu_s)\frac{\partial \bar{u}_{interface}}{\partial \bar{x}}=\beta RTc_{ref}\bar{p}_{interface} \tag{21}$$

In order to implement the transient simulation for kinetics of the electric-sensitive hydrogels, initial conditions are required. It is assumed here that initially the hydrogel is in the equilibrium state when the effect of bath solution is considered only, namely no external electric field is applied. This equilibrium state will be taken as initial condition for transient simulation. Thus corresponding steady-state computational results are used as the initial conditions as

$$\bar{c}^{transient}_{initial}=\bar{c}^{steady}_{v=0} \tag{22}$$

$$\bar{\psi}^{transient}_{initial}=\bar{\psi}^{steady}_{v=0} \tag{23}$$

$$\bar{p}^{transient}_{initial}=\bar{p}^{steady}_{v=0} \tag{24}$$

$$\bar{u}^{transient}_{initial}=\bar{u}^{steady}_{v=0} \tag{25}$$

where $\bar{c}^{steady}_{v=0}$, $\bar{\psi}^{steady}_{v=0}$, $\bar{p}^{steady}_{v=0}$ and $\bar{u}^{steady}_{v=0}$ are the steady-state simulating results without the effect of externally applied electric field.

2.3. Discretization of the transient governing equations of the MECe model

A meshless numerical method, termed the Hermite-cloud method (Li et al., 2003, 2004b), is used for transient solution of the nonlinear partial differential governing equations (14)–(17) of the MECe model. The Hermite-cloud method constructs the Hermite-type interpolation functions and employs the point collocation for discretization of the governing equations to directly compute the approximate solutions of both unknown functions and first-order derivatives (Li et al., 2003, 2004b). By the Hermite-cloud method, an unknown continuous real function $f(x,y)$ can expressed approximately by

$$\begin{aligned}\tilde{f}(x,y)=&\sum_{n=1}^{N_T}N_n(x,y)f_n+\sum_{m=1}^{N_S}\left(x-\sum_{n=1}^{N_T}N_n(x,y)x_n\right)M_m(x,y)g_{xm}\\&+\sum_{m=1}^{N_S}\left(y-\sum_{n=1}^{N_T}N_n(x,y)y_n\right)M_m(x,y)g_{ym}\end{aligned} \tag{26}$$

where $N_n(x,y)$ and $M_n(x,y)$ are defined as the shape functions of the unknown function $f(x,y)$ and corresponding first-order differential functions $g_x(x,y)$ and $g_y(x,y)$, respectively, which are simply polynomials in x and y. f_n denotes the unknown point value of $f(x,y)$ at the nth discrete point, g_{xm} and g_{ym} the unknown point values of $g_x(x,y)$ and $g_y(x,y)$ at the mth discrete point. N_T and N_S are total numbers of discrete points scattered within the computational domain.

By the θ-weighted finite difference scheme ($0.5<\theta<1.0$) (Reddy, 1993), Eq. (14) is discretized first in time t domain

$$\begin{aligned}\bar{c}^k_{(n+1)}-\bar{c}^k_{(n)}=\frac{\Delta tD_k}{L_{ref}^2}&\left[\theta\left(\frac{\partial^2 \bar{c}^k_{(n+1)}}{\partial \bar{x}^2}+\alpha z^k\frac{\partial \bar{c}^k_{(n+1)}}{\partial \bar{x}}\frac{\partial \bar{\psi}_{(n+1)}}{\partial \bar{x}}+\alpha z^k\bar{c}^k_{(n+1)}\frac{\partial^2 \bar{\psi}_{(n+1)}}{\partial \bar{x}^2}\right)\right.\\&\left.+(1-\theta)\left(\frac{\partial^2 \bar{c}^k_{(n)}}{\partial \bar{x}^2}+\alpha z^k\frac{\partial \bar{c}^k_{(n)}}{\partial \bar{x}}\frac{\partial \bar{\psi}_{(n)}}{\partial \bar{x}}+\alpha z^k\bar{c}^k_{(n)}\frac{\partial^2 \bar{\psi}_{(n)}}{\partial \bar{x}^2}\right)\right]\end{aligned} \tag{27}$$

where the subscript n denotes time $t = t_n$ and $\Delta t = t_{n+1} - t_n$ is time step. By the Hermite-cloud method (Li et al., 2003, 2004b), Eq. (27) is further discretized in spatial domain as shown in Appendix. Similarly, Eqs. (15)–(17) are also discretized in both time and spatial domains and shown in Appendix.

3. Validation of the MECe model

Computational accuracy of the MECe model for steady-state simulation has been examined for equilibrium of the electric-sensitive hydrogels (Li et al., 2004a,c). In this section, the MECe model will be further validated for transient simulation and compared with published experimental data. In terms of the experiment of the hydrogel kinetics subject to external electric field, only one study was found and done by Shiga and Kurauchi (1990). As illustrated in Fig. 2, they experimentally measured the endpoint displacement D of a hydrogel strip in a straightforward manner, instead of the displacement u at the edge point b of the present 1D computational domain between the edge points a and b in the hydrogel thickness h direction along symmetric x-axis. In other words, the experimentally measured displacement D and the computed displacement u are located in different regions of the hydrogel strip. For an approximate comparison, an analogue relation is required between the two displacements u and D at different positions of the hydrogel strip. The experimental data (Shiga and Kurauchi, 1990) used as input data for the present numerical simulation of the MECe model include $T = 298$ K, $R = 8.314$ J/mol K, $F_c = 9.648 \times 10^4$ C/mol, $\varepsilon_0 = 8.854 \times 10^{-12}$ C^2/Nm^2, $\varepsilon = 80$, $\phi_0^w = 0.8$, $c_0^f = 35.3$ mol/m^3, $z^f = -1$, $c^* = 35.3$ mol/m^3, $V_e = 3.0$ V, $3\lambda + 2\mu = 1.8 \times 10^4$ Pa, $L = 5.0 \times 10^{-2}$ m, and $h = 5.0 \times 10^{-3}$ m, which were obtained experimentally by Shiga and Kurauchi (1990). The computed displacement u and experimentally measured displacement D are tabulated at time $t = 1$, 2, 3, 4 and 5 min, respectively, as shown in Table 1. The relation between the displacements u and D is constructed as a result of using the least square technique with best fitting to the displacements u and D at time $t = 1$, 3 and 5 min only, and expressed by

$$D = 1.58 + 0.93u + 0.47u^2 \tag{28}$$

For examination of the above relation, the displacements u and D are substituted at time $t = 2$ and 4 min into Eq. (28), respectively, the relative discrepancies are computed and they are generally less than 6%. The relation (28) is thus validated acceptable. Finally, for comparison of the transient displacements D between experiment (Shiga and Kurauchi, 1990) and computation by Eq. (28), Fig. 3 is plotted and good agreement is achieved for the transient simulation. This validates the MECe model suitable for kinetics of the electric-sensitive hydrogels.

4. Simulation and discussion for parameter study of kinetics of the hydrogels

For deeper understanding of the kinetics of smart hydrogels responding to electric stimulus, numerical simulations are conducted. Several parameters, including $T = 298$ K, $R = 8.314$ J/mol K, $F_c = 9.648 \times 10^4$ C/mol, $\varepsilon_0 = 8.854 \times 10^{-12}$ C^2/Nm^2, $\varepsilon = 80$, $\phi_0^w = 0.8$, $3\lambda + 2\mu = 1.2 \times 10^5$ Pa, $f_{ws} = 7.0 \times 10^{-16}$ Ns/m^4, $D_k = 1.0 \times 10^{-7}$ m^2/s, $z^f = -1$, $L = 1.5 \times 10^{-2}$ m and $h = 5 \times 10^{-3}$ m, are taken as input data of the MECe model for the following parameter studies.

Table 1
Displacements D and u at different time.

Time (min)	1	2	3	4	5
Displacement D (mm)	2.1	3.1	4.1	5.0	6.1
Displacement u (mm)	0.45	0.97	1.54	1.94	2.27

D is the experimentally measured displacement at the endpoint of hydrogel strip. u is the displacement at the edge point a of the one-dimensional computational domain.

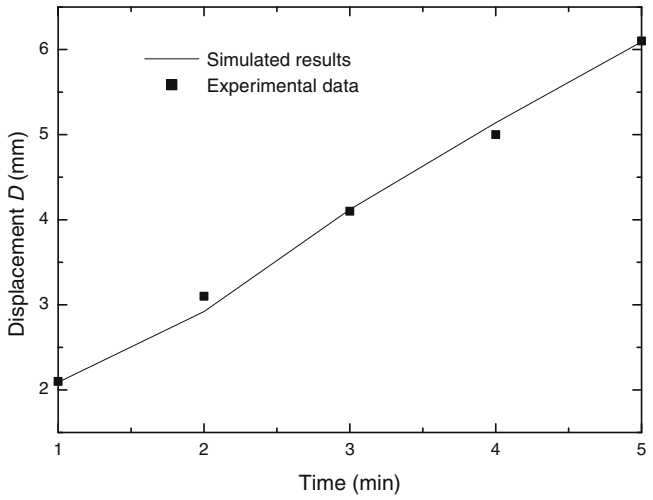

Fig. 3. Comparison between the transiently simulating results and experimental data.

4.1. Kinetics of diffusive ion concentrations

Figs. 4–7 are plotted for analysis of the kinetics of diffusive ion concentrations under different externally applied electric voltages V_e and bath solution concentrations c^* when the initially fixed-charge density $c_0^f = 2$ mol/m^3. Deformations of the electric-sensitive hydrogels with time are also presented accordingly. It is shown from these figures that the concentrations of diffusive ions are distributed symmetrically over whole computational domain at initial time $t = 0$ when no external electric field is applied, although the distributions of the diffusive ion concentrations are not exactly symmetrical due to the approximate discretization. These are achieved by the steady-state simulations as mentioned above. When the external electric voltage V_e is applied, the concentration distributions of the diffusive ionic species are no longer

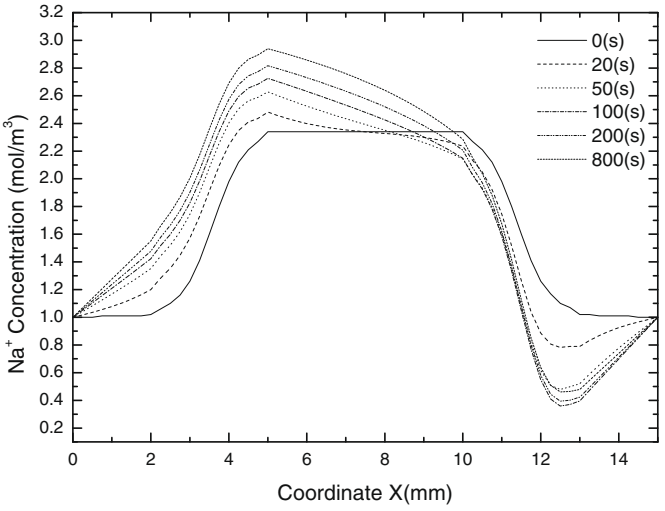

Fig. 4. Na^+ concentration kinetics when $V_e = 0.3$ V, $c_0^f = 2$ mol/m^3 and $c^* = 1$ mol/m^3.

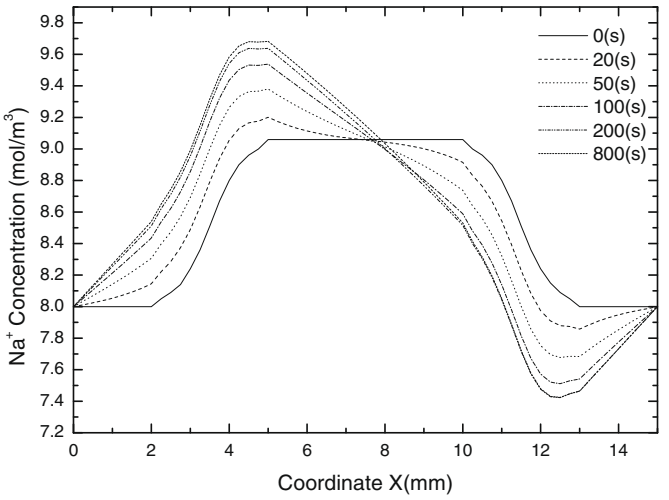

Fig. 5. Na^+ concentration kinetics when $V_e = 0.2$ V, $c_0^f = 2$ mol/m^3 and $c^* = 8$ mol/m^3.

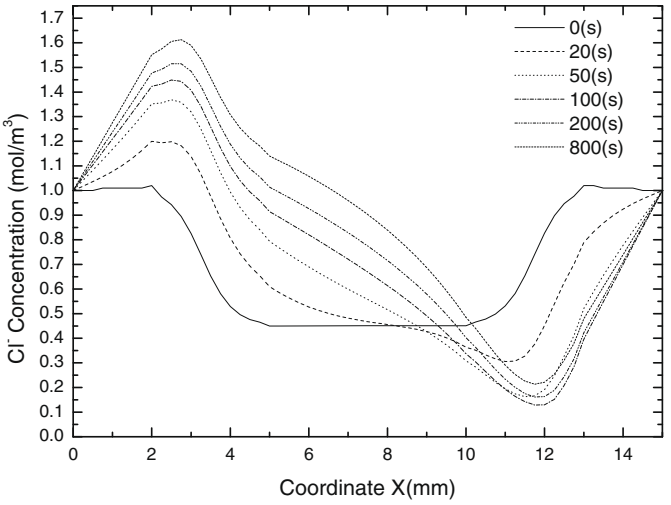

Fig. 6. Cl^- concentration kinetics when $V_e = 0.3$ V, $c_0^f = 2$ mol/m^3 and $c^* = 1$ mol/m^3.

symmetric. The concentrations of diffusive ions redistribute continuously with time in both the hydrogel and bath solution. The differences of the concentrations near the hydrogel–solution interfaces increase accordingly with time. It is predictable that the ionic diffusion and convection will reach an equilibrium state after certain time, which depends on material properties and environments such as the initially fixed-charge density c_0^f, electric voltage V_e and surrounding bath solution concentration c^*. It is found that the trends of kinetics of distributive concentrations illustrated in Figs. 4–7 are in good agreement with the FEM simulation by Wallmersperger et al. (2001, 2004).

For further analysis of the transport rate from the unsteady to equilibrium states, Figs. 4–7 are studied again in detail. The coupled influences of the externally applied electric voltage V_e and bath solution concentration c^* on the transport rate are shown in Figs. 4 and 5 for the cation Na^+, and in Figs. 6 and 7 for the anion Cl^-. For a given initially fixed-charge density $c_0^f = 2$ mol/m^3, it is seen from the figures that the transport rate increases with decreasing the electric voltage V_e or with increasing the bath solution concentration c^*. In any case however, the peak values of ionic concentrations over the hydrogel–solution interface near the cathode always increase with time t, while those near the anode always decrease with time t. As a result, the concentration differences of diffusive ion species between the two hydrogel–solution interfaces increase monotonically with time t.

4.2. Variation of distributive electric potential with time

Figs. 8 and 9 illustrate the variations of the distributive electric potential ψ with time for different externally applied electric voltages V_e and surrounding bath solution concentrations c^* when the initially fixed-charge density $c_0^f = 2$ mol/m^3. It is observed that the downward steps of distributive profiles of the electric potential ψ within hydrogels increase with time. After a time of about 100 s, the variation of the downward steps becomes gradual. The coupled influences of the environmental conditions are also found from the two figures. The downward steps of electric potential ψ profiles over the hydrogel–solution interface diminish obviously either with the increment of the bath solution concentration c^*, or with decreasing the electric voltage V_e.

4.3. Variation of distributive displacement of the hydrogel with time

Variations of the distributive displacements of the hydrogels with time are presented in Figs. 10–15 for analysis of the deforma-

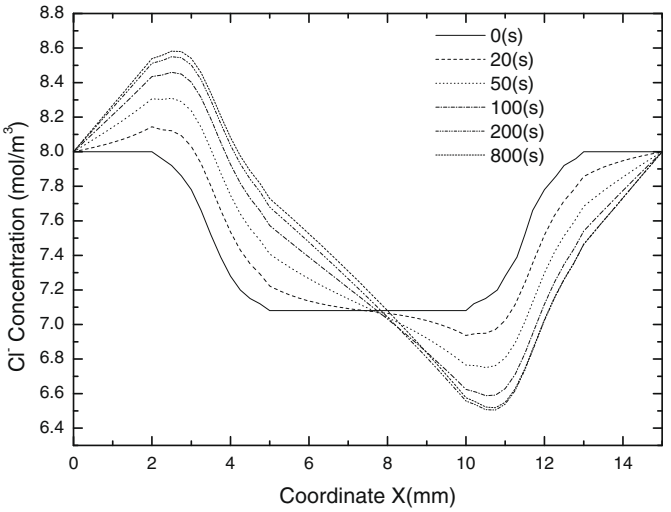

Fig. 7. Cl^- concentration kinetics when $V_e = 0.2$ V, $c_0^f = 2$ mol/m^3 and $c^* = 8$ mol/m^3.

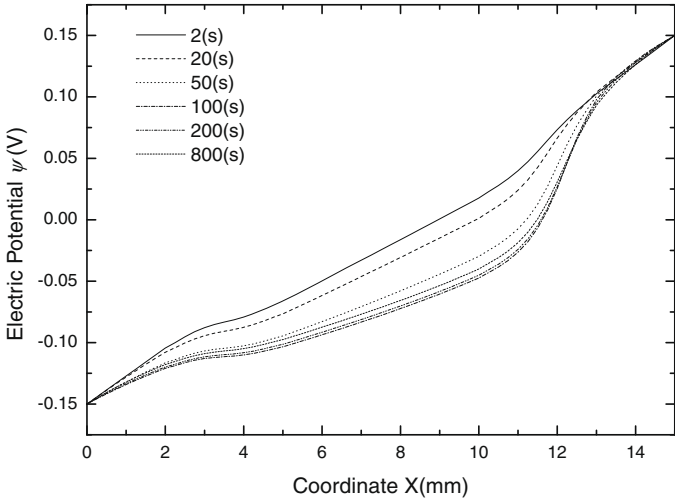

Fig. 8. Variation of electric potential with time when $V_e = 0.3$ V, $c_0^f = 2$ mol/m^3 and $c^* = 1$ mol/m^3.

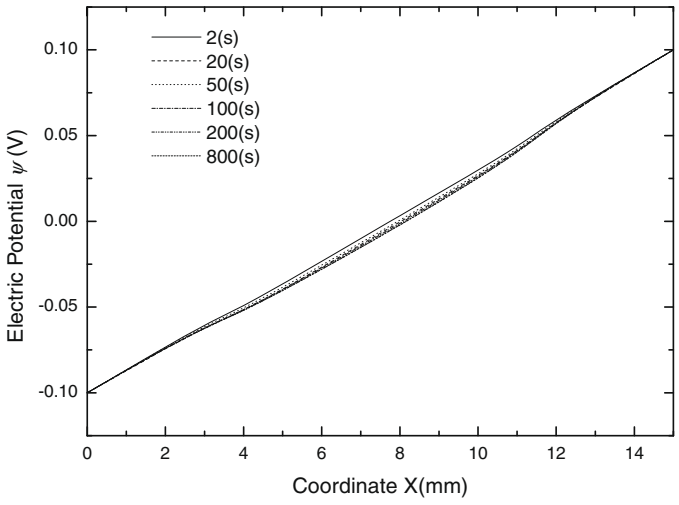

Fig. 9. Variation of electric potential with time when $V_e = 0.2$ V, $c_0^f = 2$ mol/m^3 and $c^* = 8$ mol/m^3.

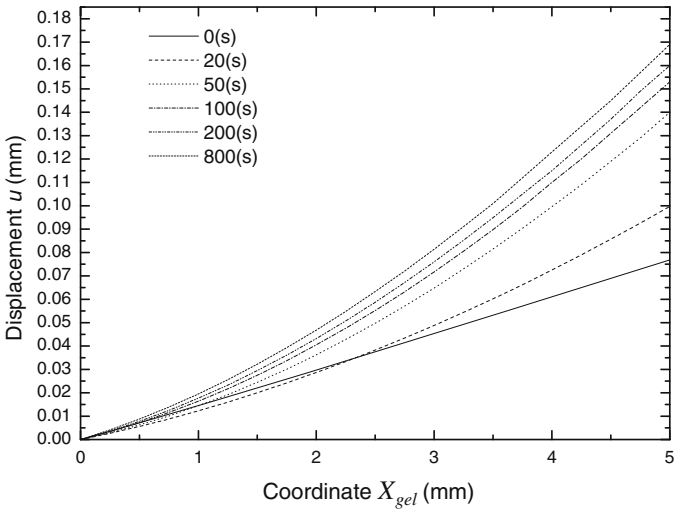

Fig. 12. Variation of displacement with time when $V_e = 0.4$ V, $c_0^f = 2$ mol/m^3 and $c^* = 1$ mol/m^3.

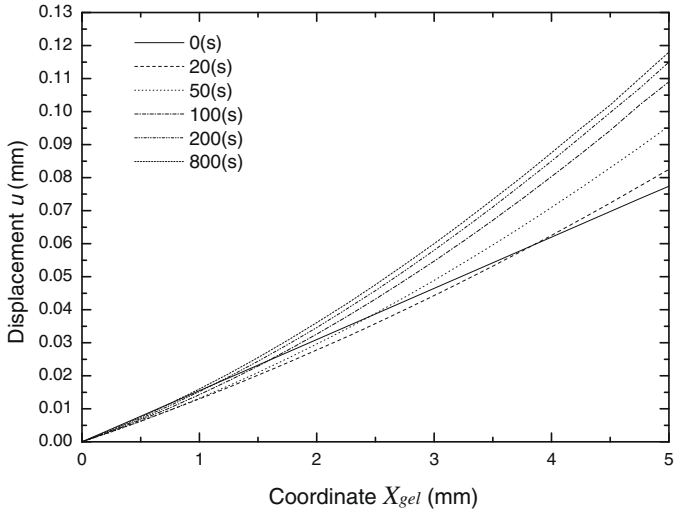

Fig. 10. Variation of displacement with time when $V_e = 0.2$ V, $c_0^f = 2$ mol/m^3 and $c^* = 1$ mol/m^3.

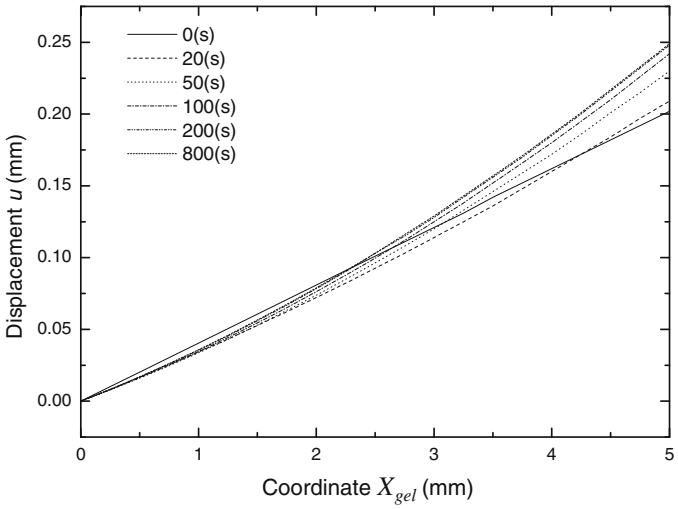

Fig. 13. Variation of displacement with time when $V_e = 0.2$ V, $c_0^f = 4$ mol/m^3 and $c^* = 1$ mol/m^3.

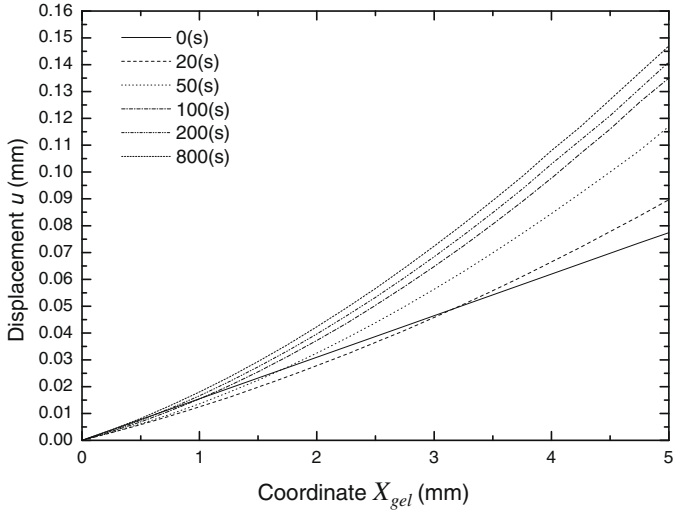

Fig. 11. Variation of displacement with time when $V_e = 0.3$ V, $c_0^f = 2$ mol/m^3 and $c^* = 1$ mol/m^3.

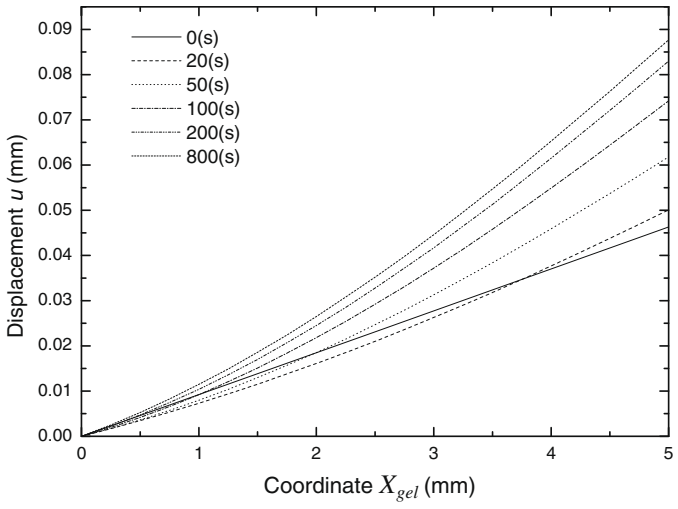

Fig. 14. Variation of displacement with time when $V_e = 0.2$ V, $c_0^f = 2$ mol/m^3 and $c^* = 2$ mol/m^3.

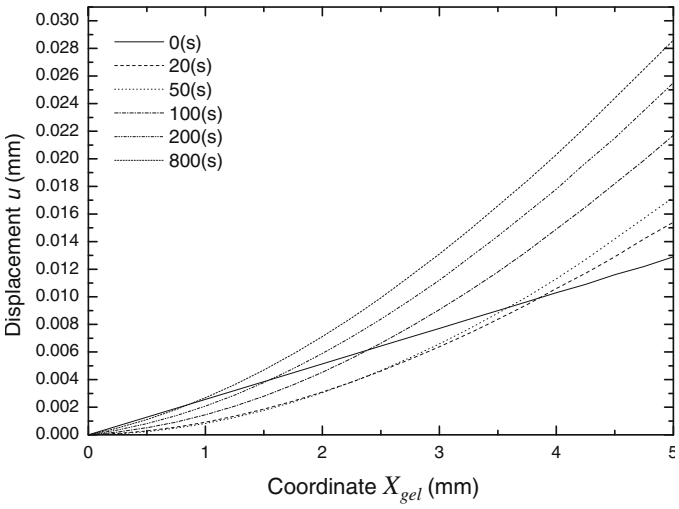

Fig. 15. Variation of displacement with time when $V_e = 0.2$ V, $c_0^f = 2$ mol/m^3 and $c^* = 8$ mol/m^3.

tion of the electric-sensitive hydrogel. It is known that the trend of variations of distributive displacements is similar to that of the distributive electric potential, and the displacement of the hydrogel increases with time. Initially the displacement increases rapidly and then gradually. It is also observed that the displacements of the hydrogels linearly distribute along the x direction before the external electric field is applied. With applied electric voltage V_e, the distributions of the displacement become more and more nonlinear. It is evidently seen from Figs. 10–15 that the distributive curves are linear at $t = 0$ and subsequently become nonlinear. One of the reasons may be that the coupled effect of chemical and electric fields appears in the considered system when the electric field is applied, and then the displacement of the hydrogel immediately demonstrates the nonlinear distribution. In addition, the influence of the externally applied electric voltage V_e on the variations of the distributive displacements of the hydrogels is shown in Figs. 10–12, in which the increment of the electric voltage V_e makes the hydrogels have larger deformation. Figs. 10–13 demonstrate the influence of the initially fixed-charge density c_0^f on the variations of the distributive displacements of the hydrogels, in which the displacements increase with the initially fixed-charge density c_0^f. The influence of the surrounding bath solution concentration c^* is illustrated in Figs. 10, 14 and 15, in which the displacements decrease with the increment of the bath solution concentration c^*. Based on the above discussions of Figs. 10–15, it is concluded that the displacement of the hydrogel first increases rapidly with time and then in a more gradual manner. Therefore, the electric-sensitive hydrogels can be designed with capability of fast responding to external electric trigger. This is an attractive feature of the electric-sensitive hydrogels used as biosensors/bioactuators for BioMEMS applications.

5. Conclusions

The transient simulation has been conducted by the MECe model for analysis of the kinetics of electric-stimulus responsive hydrogels. The model is composed of coupled nonlinear partial differential governing equations, and it has been examined for kinetic study by comparison with published experiments. The kinetics of diffusive ionic species concentration is simulated well and is good agreement with the published steady-state simulation. Influences of important parameters are discussed in detail, including the externally applied electric voltage, initially fixed-charge density and surrounding bath solution concentrations as well as the displacement of the hydrogel. By the present transient simulations, it is concluded that the smart hydrogels have the capability of responding to the externally applied electric field in short time.

Acknowledgements

The authors gratefully acknowledge the financial support from the Agency for Science, Technology and Research (A*STAR) of Singapore through A*STAR SERC Grant – SRP on MEMS Phase II under the Project No. 022 107 0009.

Appendix A. Discretization of the governing Eqs. (15)–(17) and (27)

By the Hermite-cloud method, Eq. (27) is further discretized in spatial domain as

$$\begin{aligned}
&\sum_{j=1}^{np} N_j(\bar{x}_i)\bar{c}^k_{j(n+1)} - \sum_{m=1}^{np}\left(\bar{x}_i - \sum_{j=1}^{np} N_j(\bar{x}_i)\bar{x}_j\right) M_m(\bar{x}_i)\bar{c}^k_{xm(n+1)} \\
&\quad - \frac{\Delta t D_k \theta}{L_{ref}^2}\left\{\sum_{j=1}^{np} N_{xx_j}(\bar{x}_i)\bar{c}^k_{j(n+1)} + \alpha z^k \sum_{m=1}^{np} M_m(\bar{x}_i)\bar{c}^k_{xm(n+1)}\right. \\
&\quad \times \sum_{m=1}^{np} M_m(\bar{x}_i)\bar{\psi}_{xm(n+1)} + \alpha z^k \sum_{j=1}^{np} N_{xx_j}(\bar{x}_i)\bar{\psi}_{j(n+1)} \\
&\quad \left.\times \left[\sum_{j=1}^{np} N_j(\bar{x}_i)\bar{c}^k_{j(n+1)} - \sum_{m=1}^{np}(\bar{x}_i - \sum_{j=1}^{np} N_j(\bar{x}_i)\bar{x}_j) M_m(\bar{x}_i)\bar{c}^k_{xm(n+1)}\right]\right\} \\
&= \sum_{j=1}^{np} N_j(\bar{x}_i)\bar{c}^k_{j(n)} - \sum_{m=1}^{np}\left(\bar{x}_i - \sum_{j=1}^{np} N_j(\bar{x}_i)\bar{x}_j\right) M_m(\bar{x}_i)\bar{c}^k_{xm(n)} \\
&\quad + \frac{\Delta t D_k (1-\theta)}{L_{ref}^2}\left\{\sum_{j=1}^{np} N_{xx_j}(\bar{x}_i)\bar{c}^k_{j(n)} + \alpha z^k \sum_{m=1}^{np} M_m(\bar{x}_i)\bar{c}^k_{xm(n)}\right. \\
&\quad \times \sum_{m=1}^{np} M_m(\bar{x}_i)\bar{\psi}_{xm(n)} + \alpha z^k \left[\sum_{j=1}^{np} N_j(\bar{x}_i)\bar{c}^k_{j(n)} - \sum_{m=1}^{np}(\bar{x}_i\right. \\
&\quad \left.\left. - \sum_{j=1}^{np} N_j(\bar{x}_i)\bar{x}_j) M_m(\bar{x}_i)\bar{c}^k_{xm(n)}\right] \sum_{j=1}^{np} N_{xx_j}(\bar{x}_i)\bar{\psi}_{j(n)}\right\}
\end{aligned} \tag{A1}$$

Eqs. (15)–(17) are also discretized similarly in both time and spatial domains as follows:

$$\begin{aligned}
&\sum_{j=1}^{np} N_{xx_j}(\bar{x}_i)\bar{\psi}_{j(n+1)} + \frac{F_c^2 L_{ref}^2 c_{ref}}{\varepsilon\varepsilon_0 RT\alpha}\left\{z^f \bar{c}^f + \sum_{k=+,-} z^k \left[\sum_{j=1}^{np} N_j(\bar{x}_i)\bar{c}^k_{j(n+1)}\right.\right. \\
&\quad \left.\left. - \sum_{m=1}^{np}(\bar{x}_i - \sum_{j=1}^{np} N_j(\bar{x}_i)\bar{x}_j) M_m(\bar{x}_i)\bar{c}^k_{xm(n+1)}\right]\right\} = 0
\end{aligned} \tag{A2}$$

$$(3\lambda_s + 2\mu_s)\sum_{j=1}^{npGel} N_{xx_j}(\bar{x}_i)\bar{u}_{j(n+1)} - \beta RT c_{ref}\sum_{m=1}^{npGel} M_m(\bar{x}_i)\bar{p}_{xm(n+1)} = 0 \tag{A3}$$

$$\begin{aligned}
&\frac{L_{ref}^2 f_{ws}}{c_{ref}RT}\sum_{m=1}^{npGel} M_m(\bar{x}_i)\bar{u}_{xm(n+1)} \\
&\quad - \Delta t\theta\beta\left[\phi^w \sum_{j=1}^{npGel} N_{xx_j}(\bar{x}_i)\bar{p}_{j(n+1)} + 2\frac{\partial\phi^w}{\partial\bar{x}}\sum_{m=1}^{npGel} M_m(\bar{x}_i)\bar{p}_{xm(n+1)}\right] \\
&\quad - \alpha\Delta t\theta\left\{2\frac{\partial\phi^w}{\partial\bar{x}}\left[\sum_{m=1}^{npGel} M_m(\bar{x}_i)\bar{\psi}_{xm(n+1)}\right]\left[\sum_{k=+,-} z^k \sum_{j=1}^{npGel}\left(N_j(\bar{x}_i)\bar{c}^k_{j(n+1)}\right.\right.\right. \\
&\quad \left.\left.\left. - \sum_{m=1}^{npGel}\left(\bar{x}_i - \sum_{j=1}^{npGel} N_j(\bar{x}_i)\bar{x}_j\right) M_m(\bar{x}_i)\bar{c}^k_{xm(n+1)}\right)\right]
\end{aligned}$$

$$+\phi^w\left[\sum_{m=1}^{npGel} M_m(\bar{x}_i)\bar{\psi}_{xm(n+1)}\left(\sum_{k=+,-} z^k \sum_{m=1}^{npGel} M_m(\bar{x}_i)\bar{c}^k_{xm(n+1)}\right)+\sum_{j=1}^{npGel} N_{xx_j}(\bar{x}_i)\bar{\psi}_{j(n+1)}\right.$$
$$\left.\times\sum_{k=+,-} z^k \sum_{j=1}^{npGel}\left(N_j(\bar{x}_i)\bar{c}^k_{j(n+1)}-\sum_{m=1}^{npGel}\left(\bar{x}_i-\sum_{j=1}^{npGel} N_j(\bar{x}_i)\bar{x}_j\right)M_m(\bar{x}_i)\bar{c}^k_{xm(n+1)}\right)\right]\Bigg\}$$
$$=\frac{L^2_{ref}f_{ws}}{c_{ref}RT}\sum_{m=1}^{npGel} M_m(\bar{x}_i)\bar{u}_{xm(n)}+\Delta t(1-\theta)\beta\left[\phi^w\sum_{j=1}^{npGel} N_{xx_j}(\bar{x}_i)\bar{p}_{j(n)}\right.$$
$$\left.+2\frac{\partial\phi^w}{\partial\bar{x}}\sum_{m=1}^{npGel} M_m(\bar{x}_i)\bar{p}_{xm(n)}\right]+\alpha\Delta t(1-\theta)\left\{2\frac{\partial\phi^w}{\partial\bar{x}}\left[\sum_{m=1}^{npGel} M_m(\bar{x}_i)\bar{\psi}_{xm(n)}\right]\right.$$
$$\left.\times\left[\sum_{k=+,-} z^k\sum_{j=1}^{npGel}\left(N_j(\bar{x}_i)\bar{c}^k_{j(n)}-\sum_{m=1}^{npGel}\left(\bar{x}_i-\sum_{j=1}^{npGel} N_j(\bar{x}_i)\bar{x}_j\right)M_m(\bar{x}_i)\bar{c}^k_{xm(n)}\right)\right]\right.$$
$$+\phi^w\left[\sum_{m=1}^{npGel} M_m(\bar{x}_i)\bar{\psi}_{xm(n)}\left(\sum_{k=+,-} z^k\sum_{m=1}^{npGel} M_m(\bar{x}_i)\bar{c}^k_{xm(n)}\right)+\sum_{j=1}^{npGel} N_{xx_j}(\bar{x}_i)\bar{\psi}_{j(n)}\right.$$
$$\left.\left.\times\sum_{k=+,-} z^k\sum_{j=1}^{npGel}\left(N_j(\bar{x}_i)\bar{c}^k_{j(n)}-\sum_{m=1}^{npGel}\left(\bar{x}_i-\sum_{j=1}^{npGel} N_j(\bar{x}_i)\bar{x}_j\right)M_m(\bar{x}_i)\bar{c}^k_{xm(n)}\right)\right]\right\} \quad (A4)$$

By the Hermite theorem (Li et al., 2003, 2004b), the following auxiliary equations are required,

$$\sum_{j=1}^{np} N_{xj}(\bar{x}_i)\bar{c}^k_{j(n+1)}-\left[\sum_{j=1}^{np} N_{xj}(\bar{x}_i)\bar{x}_j\right]\sum_{m=1}^{np} M_m(\bar{x}_i)\bar{c}^k_{xm(n+1)}=0 \quad (A5)$$

$$\sum_{j=1}^{np} N_{xj}(\bar{x}_i)\bar{\psi}_{j(n+1)}-\left[\sum_{j=1}^{np} N_{xj}(\bar{x}_i)\bar{x}_j\right]\sum_{m=1}^{np} M_m(\bar{x}_i)\bar{\psi}_{xm(n+1)}=0 \quad (A6)$$

$$\sum_{j=1}^{npGel} N_{xj}(\bar{x}_i)\bar{u}_{j(n+1)}-\left[\sum_{j=1}^{npGel} N_{xj}(\bar{x}_i)\bar{x}_j\right]\sum_{m=1}^{npGel} M_m(\bar{x}_i)\bar{u}_{xm(n+1)}=0 \quad (A7)$$

$$\sum_{j=1}^{npGel} N_{xj}(\bar{x}_i)\bar{p}_{j(n+1)}-\left[\sum_{j=1}^{npGel} N_{xj}(\bar{x}_i)\bar{x}_j\right]\sum_{m=1}^{npGel} M_m(\bar{x}_i)\bar{p}_{xm(n+1)}=0 \quad (A8)$$

References

Beebe, D.J., Moore, J., Bauer, J.M., Yu, Q., Liu, R.H., Devadoss, C., Jo, B.H., 2000. Functional structures for autonomous flow control inside micro-fluidic channels. Nature 404, 588–590.

Chen, G., Hoffman, A.S., 1995. Graft copolymers that exhibit temperature-induced phase transitions over a wide range of pH. Nature 373, 49–52.

Eisenberg, S.R., Grodzinsky, A.J., 1987. The kinetics of chemically induced nonequilibrium swelling of articular cartilage and corneal stroma. ASME Journal of Biomechanical Engineering 109, 79–89.

Galaev, I.Y., Mattiasson, B., 1999. 'Smart' polymers and what they could do in biotechnology and medicine. Trends in Biotechnology 17, 335–340.

Jeong, B., Gutowska, A., 2002. Lessons from nature: stimuli-responsive polymers and their biomedical applications. Trends in Biotechnology 20, 305–311.

Kataoka, K., Miyazaki, H., Bunya, M., Okano, T., Sakurai, Y., 1998. Totally synthetic polymer gels responding to external glucose concentration: their preparation and application to on–off regulation of insulin release. Journal of the American Chemical Society 120, 12694–12695.

Kokufuta, E., Zhang, Y.Q., Tanaka, T., 1991. Saccharide-sensitive phase transition of a lectin-loaded gel. Nature 351, 302–304.

Kwon, I.C., Bae, Y.H., Kim, S.W., 1991. Electrically erodible polymer gel for controlled release of drugs. Nature 354, 291–293.

Lai, W.M., Hou, J.S., Mow, V.C., 1991. A triphasic theory for the swelling and deformation behaviors of articular cartilage. ASME Journal of Biomechanical Engineering 113, 245–258.

Lanir, Y., 1987. Biorheology and fluid flux in swelling tissues I. Biocomponent theory for small deformations, including concentration effects. Biorheology 23, 173–188.

Li, H., Chen, J., Lam, K.Y., 2004a. Multiphysic modeling and meshless simulation of electric-sensitive hydrogels. Journal of Polymer Science: Part B: Polymer Physics 42, 1514–1531.

Li, H., Cheng, J.Q., Ng, T.Y., Chen, J., Lam, K.Y., 2004b. A meshless Hermite-cloud method for nonlinear fluid structure analysis of near-bed submarine pipelines under current. Engineering Structures 26, 531–542.

Li, H., Luo, R.M., Birgersson, E., Lam, K.Y., 2007. Modeling of multiphase smart hydrogels responding to pH and electric voltage coupled stimuli. Journal of Applied Physics 101, 114905.

Li, H., Ng, T.Y., Cheng, J.Q., Lam, K.Y., 2003. Hermite-cloud: a novel true meshless method. Computational Mechanics 33, 30–41.

Li, H., Yuan, Z., Lam, K.Y., Lee, H.P., Chen, J., Hanes, J., Fu, J., 2004c. Model development and numerical simulation of electric-stimulus-responsive hydrogels subject to an externally applied electric field. Biosensors and Bioelectronics 19, 1097–1107.

Mow, V.C., Kuei, S.C., Lai, W.M., Armstrong, C.G., 1980. Biphasic creep and stress relaxation of articular cartilage in compression: theory and experiments. ASME Journal of Biomechanical Engineering 102, 73–84.

Myers, E.R., Lai, W.M., Mow, V.C., 1984. A continuum theory and an experiment for the ion-induced swelling behavior of articular cartilage. ASME Journal of Biomechanical Engineering 106, 151–158.

Osada, Y., Okuzaki, H., Hori, H., 1992. A polymer gel with electrically driven motility. Nature 355, 242–244.

Reddy, J.N., 1993. An Introduction to the Finite Element Method. McGraw-Hill, New York. p. 227.

Shiga, T., Kurauchi, T., 1990. Deformation of polyelectrolyte gels under the influence of electric field. Journal of Applied Polymer Science 39, 2305–2320.

Siegel, R.A., Firestone, B.A., 1988. pH-dependent equilibrium swelling properties of hydrophobic polyelectrolyte copolymer gels. Macromolecules 21, 3254–3259.

Tanaka, T., 1978. Collapse of gels and the critical endpoint. Physical Review Letters 40, 820–823.

Tanaka, T., Fillmore, D., Sun, S.T., Nishio, I., Swislow, G., Shah, A., 1980. Phase transitions in ionic gels. Physical Review Letters 45, 1636–1639.

Tanaka, T., Nishio, I., Sun, S.T., Ueno-Nishio, S., 1982. Collapse of gels in an electric field. Science 218, 467–469.

Wallmersperger, T., Kröplin, B., Gülch, R.W., 2004. Coupled chemo-electro-mechanical formulation for ionic polymer gels – numerical and experimental investigations. Mechanics of Materials 36, 411–420.

Wallmersperger, T., Kröplin, B., Holdenried, J., Gülch, R.W., 2001. A coupled multi-field formulation for ionic polymer gels in electric fields. In: Bar-Cohen, Y. (Ed.), SPIE Proceedings of Smart Structures and Materials 2001: Electroactive Polymer Actuators and Devices, Newport Beach, CA, USA, vol. 4329, pp. 264–275.

Yoshida, R., Uchida, K., Kaneko, Y., Sakai, K., Kikuchi, A., Sakurai, Y., Okano, T., 1995. Comb-type grafted hydrogels with rapid de-swelling response to temperature changes. Nature 374, 240–242.

Zhou, X., Hon, Y.C., Sun, S., Mak, A.F.T., 2002. Numerical simulation of the steady-state deformation of a smart hydrogel under an external electric field. Smart Materials and Structures 11, 459–467.